# Influence of precursor chemistry on CVD grown TiO$_2$ coatings: differential cell growth and biocompatibility†

Jessica Altmayer,[a] Sven Barth*[b] and Sanjay Mathur*[ac]

Nanocrystalline titanium oxide (TiO$_2$) coatings with different phases and surface topographies were deposited using chemical vapor deposition (CVD) of different homo- and heteroleptic titanium precursors of general formula [XTi(O$^i$Pr)$_3$] (X = Cl (**1**), –NEt$_2$ (**2**), –N(SiMe$_3$)$_2$ (**3**), –C$_5$H$_5$ (**4**), –O$^i$Pr (**5**) and –O$^t$Bu (**6**)) to elucidate the influence of molecular configuration on resulting material properties. The interdependence of precursor chemistry and materials features of the CVD deposits was verified by performing film growth under similar conditions using different precursor molecules (**1–6**). Studies on composition (XPS), structure (SEM, XRD) and bio-functional properties (cell tests) revealed that the decomposition process is markedly influenced by the auxiliary ligands, which led to incorporation of heteroelements (Si, Cl, N) in the films. Cell tests performed to evaluate the biocompatibility of the coatings towards the growth of bone cells showed a pronounced correlation between cell adhesion and surface morphology as well as the chemical composition. Growth of osteoblast cells was strongly enhanced on films obtained using [Ti(O$^i$Pr)$_4$] and [CpTi(O$^i$Pr)$_3$], whereas TiO$_2$ coatings produced by [ClTi(O$^i$Pr)$_3$] significantly inhibited the cell growth and their proliferation due to Cl contamination. Also, the nanomorphological features of the films were found to stimulate the cell adhesion and growth.

## Introduction

Semiconductor metal oxides display interesting functional properties subject to their crystal structure and chemical composition.[1] Among them, titanium dioxide has been widely investigated in particle and thin film forms, mainly due to its high dielectric constant (useful in microelectronic devices),[2] optical transmittance,[3] high refractive index,[4] chemical stability and photocatalytic properties ($E_g$ = 3.0–3.2 eV).[5,6] The effect of crystal structure and morphology of TiO$_2$ coatings on the functional properties such as catalytic and bioactive behaviour and switchable hydrophilicity is described in the literature.[7–9]

The good biocompatibility of titanium implants responsible for their better osseointegration is due to a well-adhered layer of native oxide, which imparts good corrosion resistance to the metallic components in the physiological environment.[10a,b] Since the native oxide layer is not homogeneous and chemically undefined (TiO$_x$(OH)$_{2−x}$), it reacts with the body fluid, releasing metal ions and material debris in the body, which is manifested in

aseptic loosening of the prosthesis. A number of recent reports have shown that nanostructured TiO$_2$ surfaces enhance biomimetic growth of apatite and are also suitable for the grafting of proteins and immobilisation of active drug components.[10c,d]

Further, the biocompatibility of the implant material can be enhanced by depositing well-defined titania coatings, whereby the film thickness, topography, surface defects, micro-nanostructure and phase as well as chemical composition play a decisive role in determining the specific bioresponse and cytotoxicity.[11–16]

Recent studies have shown that cell–surface interactions are drastically affected by surface roughness even in the subnanometer range, and minute variations in local chemical composition of films, thus challenging the established coating techniques to deliver nanostructured surfaces with homogeneous topography and surface chemistry.[17–20] In this context, molecule-based chemical vapor deposition of thin oxide films offers superior potential for coating applications as it enables the achievement of a high deposition rate, composition control and in particular, phase-selective deposition of highly pure coatings, giving it a competitive edge against physical coating techniques.[21–23] However the molecule-based chemical vapor deposition process relies on the availability of suitable precursors with tailored properties, such as volatility, desired for efficient gas phase transport, and appropriate thermal lability for chemically controlled decomposition pathways. For instance, the CVD of TiCl$_4$ require high temperatures (>800 °C) for the formation of TiO$_2$, which

*[a]Leibniz-Institute for New Materials (INM), D-66123 Saarbruecken, Germany.*
*[b]Institute of Materials Chemistry, Vienna University of Technology, A-1060 Vienna, Austria. E-mail: sven.barth@tuwien.ac.at; Fax: +43 1 5880116599; Tel: +43 1 58801165207*
*[c]Institute of Inorganic Chemistry, University of Cologne, D-50939 Cologne, Germany. E-mail: sanjay.mathur@uni-koeln.de; Fax: +49 221 470 4899; Tel: +49 221 470 5627*

† Electronic supplementary information (ESI) available: NMR data of alkoxide species, XPS data of deposits using [(Me$_3$Si)$_2$NTi(O$^i$Pr)$_3$], additional SEM images of coatings and optical images of cell tests. See DOI: 10.1039/c3ra00050h

restricts the choice of substrate materials, and also, chlorine contamination in the films is inevitable.[24,25] We report herein the synthesis of a new family of precursor molecules for the CVD of $TiO_2$ films and investigate the precursor chemistry–material properties interplay in terms of the elemental composition, phase structure and biocompatibility assessed by studying cell growth and differentiation behaviour on different films.

## Experimental

### Synthesis of precursors

Synthesis and manipulation of all compounds were performed using modified Stock's techniques, taking stringent precautions against atmospheric moisture. Solvents were purified using standard procedures and stored over molecular sieves.[26]

[$Ti(O^iPr)_4$] and [$ClTi(O^iPr)_3$] were purchased from Aldrich and purified by distillation at 55 °C/$10^{-2}$ Torr and 60 °C/$10^{-2}$ Torr, respectively. The heteroleptic precursors [$Et_2NTi(O^iPr)_3$], [$(Me_3Si)_2NTi(O^iPr)_3$], [$CpTi(O^iPr)_3$] and [$Bu^tOTi(O^iPr)_3$] were synthesized *via* metathesis reactions of [$ClTi(O^iPr)_3$] with lithium diethylamide, lithium hexamethyldisilazane, sodium cyclopentadienylide and potassium *tert*-butoxide respectively. The obtained compounds were isolated by filtration of the accrued alkali metal halide. Removal of the reaction medium (toluene) and subsequent distillation under reduced pressure ($10^{-2}$ Torr) at 75 °C [$Et_2NTi(O^iPr)_3$], at 84 °C [$(Me_3Si)_2NTi(O^iPr)_3$], at 62 °C [$CpTi(O^iPr)_3$] and at 50 °C [$Bu^tOTi(O^iPr)_3$], respectively, produced pure compounds in high yields (>80%). A generic scheme illustrating the different ligand modifications and resulting heteroleptic alkoxide species is given in Fig. 1.

All the new heteroleptic derivatives were characterized by recording ^{1}H and ^{13}C NMR spectra in benzene-$d_6$ on a Bruker NMR spectrometer AC 200. The characteristic signals of the ligands and corresponding chemical shifts are summarized in Table S1 (ESI†).

### Chemical vapor deposition and film characterization

Titania films were grown on Si(100) substrates in a horizontal cold-wall CVD reactor operating under reduced pressure ($10^{-4}$ Torr) in the temperature range 450–750 °C. The precursors were introduced in the chamber using their inherent vapor pressure, achieved by maintaining the reservoirs at appropriate temperatures (25 °C: [$ClTi(O^iPr)_3$], [$Ti(O^iPr)_4$] or

[$Bu^tOTi(O^iPr)_3$] and 45 °C: [$CpTi(O^iPr)_3$], [$Et_2NTi(O^iPr)_3$] or [$(Me_3Si)_2NTi(O^iPr)_3$]). Usual experiments were conducted using 1 ml of the respective liquid precursor species and growth duration of 30–60 min. Time-dependent evolution of volatile by-products formed during the decomposition of the precursor molecules was monitored using an on-line quadrupole mass spectrometer attached to the CVD reactor.

Surface morphology and elemental distribution were recorded with a scanning electron microscope, JSM-6400F (JEOL) coupled with an energy dispersive X-ray facility (EDX). The phase characterization and texture analysis of the CVD deposits was carried out by X-ray diffraction (XRD) analysis using a Siemens D-500 diffractometer operating with Cu-Kα radiation. X-ray photoelectron spectra were recorded on a Surface Science Instrument SSI-M-Probe using Al Kα radiation. The data were charge referenced to C 1s at the binding energy of 284 eV.

### Cell differentiation studies on titania films

The cell line (osteoblasts, MC3T3-E1 from DMSZ) used in this study was cultivated in the laboratory and exposed to various $TiO_2$ coated substrates, exhibiting different morphologies and chemical compositions. Prior to cell tests, the samples were washed, followed by sterilization in ultra-pure water and transferred to well-plates where they were loaded with the cell suspension (1 ml suspension contained approximately 70 000 cells). After an incubation time of 48 h (37 °C and 5% $CO_2$), the cells were marked with fluorescent dyes using 4′,6-diamidino-2′-phenylindole dihydrochloride (Roche, Mannheim) and Alexa Fluor 488 phalloidin (Molecular Probes, Eugene, Oregon, USA) for the cell nucleus and cytoskeleton, respectively. Optical microscopy images (Axio Vert, Zeiss; camera: Leica) of stained cells were recorded to obtain information about the cell vitality on different $TiO_2$ coated substrates. Several samples of each type (4–6 substrates) were tested in these procedures to ensure reproducibility of results obtained in these studies.

## Results and discussion

The new ligand modified compounds **1–6** are all liquids and showed high vapor pressure, and gas phase stability enabling adequate feedstock in the gas phase and an intact transfer to the substrate. The presence of pre-organized Ti–O modular units in the compounds qualify them as efficient single-source precursors especially in view of the fact that no additional source of oxygen (*e.g.*, as carrier or reactive gas) was used during the film growth and the oxygen required for the formation of $TiO_2$ was solely delivered by the molecular species. The systematic replacement of one of the alkoxo-groups with hetero-ligands changed the Ti : O ratio (1 : 3), when compared to the parent compound ([$Ti(O^iPr)_4$], 1 : 4) and also modulated the reactivity pattern and gas-phase chemistry. Given the differential bond strengths of Ti–O and Ti–Cl(N, C) units, the ligand elimination can be envisaged to be different in homoleptic and heteroleptic complexes, which ultimately determines both gas-phase and heterogeneous
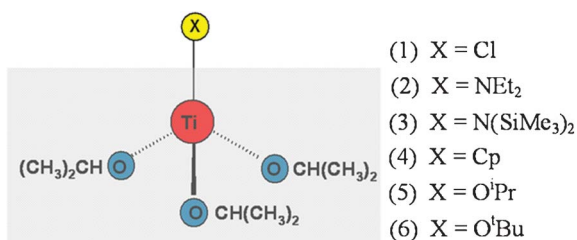


**Fig. 1** Illustration of the titanium alkoxide species used in this study.

(1) X = Cl
(2) X = NEt₂
(3) X = N(SiMe₃)₂
(4) X = Cp
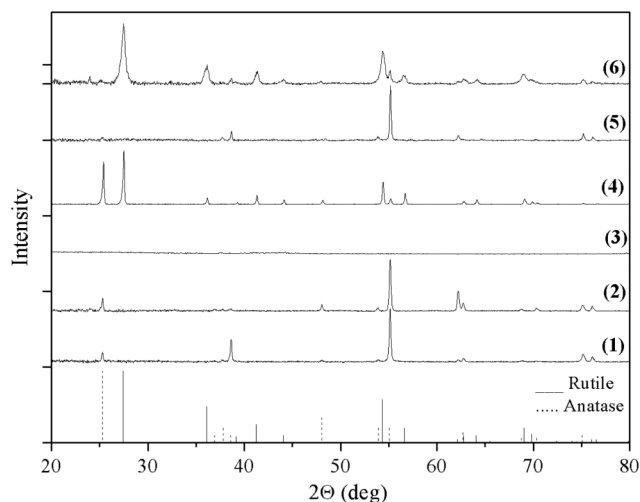(5) X = O$^i$Pr
(6) X = O$^t$Bu

**Fig. 2** X-ray diffractograms of CVD deposits obtained from the decomposition of titanium alkoxides **1–6** on Si substrates at 550 °C (reference pattern: rutile [21–1276]; anatase [21–1272]).

nucleation behaviours as supported by the substantially different surface topographies of the titania films deposited under similar conditions using different precursors. For instance, the X-ray diffraction patterns of films deposited at 550 °C on Si(100) using the precursor systems **1–6** showed significant differences in phase composition (Fig. 2).

The phase analysis revealed that CVD of $[ClTi(O^iPr)_3]$, $[Ti(O^iPr)_4]$ and $[Et_2NTi(O^iPr)_3]$ produced monophasic anatase deposits at 550 °C, whereas co-existence of rutile and anatase polymorphs was observed in the case of $[CpTi(O^iPr)_3]$ and $[Bu^tOTi(O^iPr)_3]$. On the contrary, only amorphous films were obtained using $[(Me_3Si)_2NTi(O^iPr)_3]$, even at much higher temperatures (up to 750 °C). An overview of the phase evolution and the corresponding morphologies using **1–4** at 550 °C is summarized in Fig. 3.

Interestingly, CVD of $[CpTi(O^iPr)_3]$ (Cp = $-C_5H_5$) enabled phase-selective growth of pure anatase and rutile phases at 450 °C and 650 °C, respectively. Lower carbon contamination in

these films and formation of pure TiO$_2$ phases indicated clean ligand stripping of the cyclopentadienyl group. The thermally labile nature of metal–cyclopentadienyl bonding interactions, which leads to an efficient decomposition of M–Cp units has been used to grow single crystalline Ge nanowires at very low temperatures, whereas the presence of hexamethyldisilazane ($-N(SiMe_3)_2$) units instead of Cp ligands in $[Ge\{N(SiMe_3)_2\}]$ produced Ge nanowires with a –Si–C–N shell.[27] In contrast to all other precursors, $[(Me_3Si)_2NTi(O^iPr)_3]$ produced only amorphous TiO$_2$ deposits, independent of the chosen deposition temperature (450–750 °C) and precursor flux. The X-ray photoelectron spectra of these coatings at 650 °C (Fig. S1, ESI†) showed the presence of Ti, O, C and Si with a small amount of N (2.09 at %). The elemental composition upon Ar$^+$ sputtering reveals a higher nitrogen content in the film compared to the surficial composition (N: 6.28 at %). The incorporation of N and Si, verified by the chemical composition of the precursor and chemical analyses of CVD deposits (XPS), apparently inhibit the grain growth. Also, formation of glassy phases at the grain boundaries cannot be ruled out. Higher substrate temperatures reduced the incorporation of heteroatoms as shown by XPS analysis (450 °C: N: 2.68%; Si: 7.59% and 750 °C: N: 2.46%; Si: 2.33%), but did not induce crystallisation. Pure anatase deposits were obtained using $[Ti(O^iPr)_4]$ in the temperature range 450–550 °C, whereas a mixture of anatase and rutile co-existed at higher temperatures (up to 750 °C) as previously reported in the literature.[28]

The morphology of anatase films obtained using $[ClTi(O^iPr)_3]$ strongly depended on the deposition temperature. For instance, anatase coatings deposited at 450 °C revealed larger and denser crystallites, whereas deposition at 550 °C and 650 °C produced elongated grains with pronounced faceted morphologies (Fig. 4). These surfaces are of potential interest for photo-electrochemical applications, which will be described in detail elsewhere. When compared to $[ClTi(O^iPr)_3]$, the lateral density of anatase crystallites formed under similar conditions is much higher for $[Et_2NTi(O^iPr)_3]$ (Fig. S2, ESI†). The film growth in all the cases was dominated by surface reactions that could be augmented by increasing substrate temperature. Accordingly, formation of larger crystallites was invariably observed at higher deposition temperature for all the precursors except $[(Me_3Si)_2NTi(O^iPr)_3]$ which produced smooth films constituted of globular particles (Fig. S4, ESI†) that did not exhibit any temperature-dependent change in their morphological features.

A predominant influence of precursor chemistry on the film morphology was evident in comparing the pure anatase films deposited at 450 °C using $[ClTi(O^iPr)_3]$ and $[CpTi(O^iPr)_3]$ (Table 1 and Fig. 4 and 5). Film growth using $[CpTi(O^iPr)_3]$ showed a linear relationship between film growth rates the substrate temperatures in the range 450–750 °C, however phase-selectvity was lost at higher temperature (>500 °C) resulting in mixed-phase compositions shown (Fig. 5). The homogeneous morphology formed by individual crystallites at 450 °C can be attributed to a high density of nucleation sites formed during the deposition and lower mobility of adatoms.
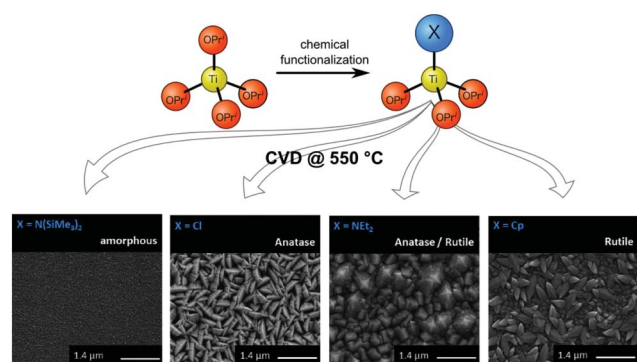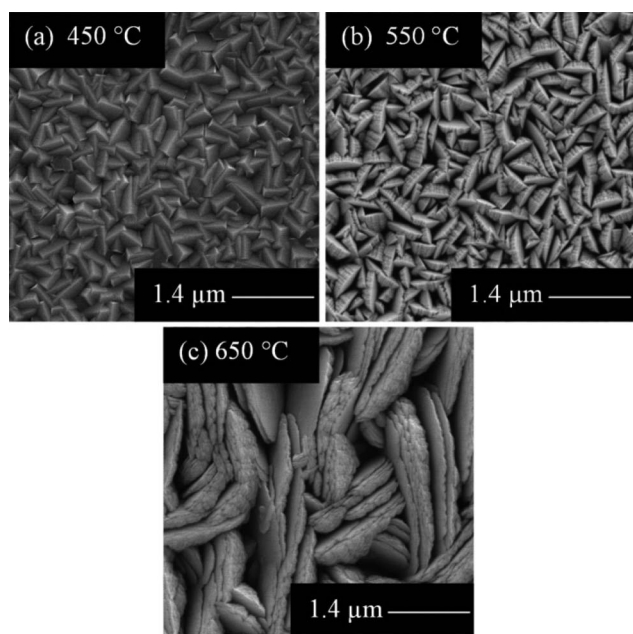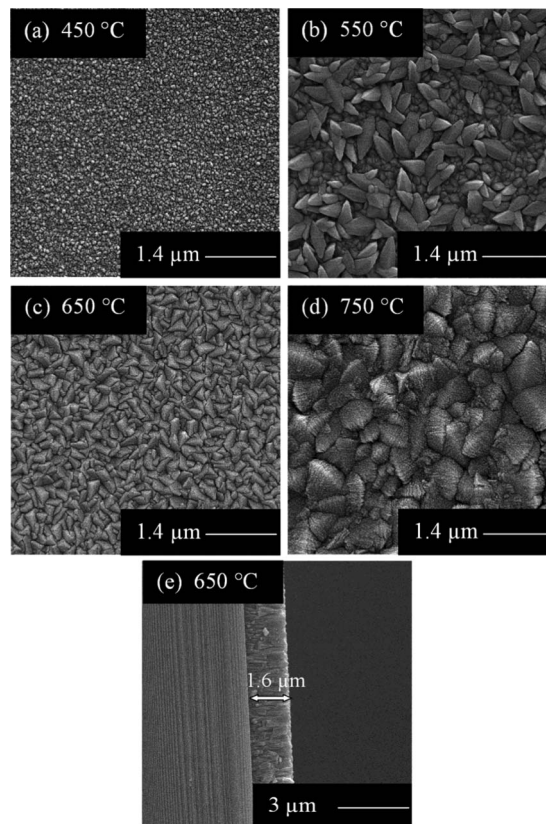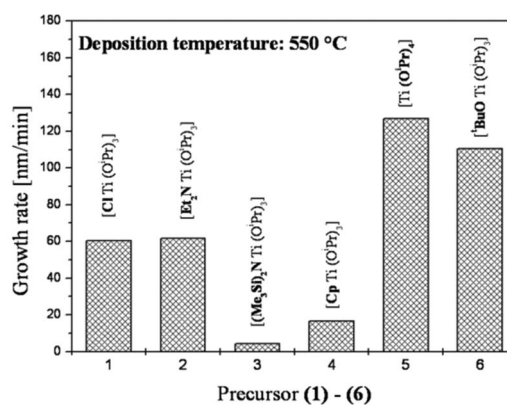


**Fig. 3** SEM images illustrating the influence of precursor chemistry on phase and morphology of TiO$_2$ films deposited under similar CVD process parameters and temperature (550 °C).

**Table 1** Overview showing the different TiO$_2$ phases obtained in the temperature range 450–750 °C.

| Precursor | Molecular units | Phase | Growth temperature |
|---|---|---|---|
| [ClTi(O$^i$Pr)$_3$] | Ti–O and Ti–Cl | Anatase | 450 °C |
| | | | 550 °C |
| | | | 650 °C |
| [Et$_2$NTi(O$^i$Pr)$_3$] | Ti–O and Ti–N | Anatase | 450 °C |
| | | | 550 °C |
| | | Anatase–rutile | 650 °C |
| | | | 750 °C |
| [(Me$_3$Si)$_2$NTi(O$^i$Pr)$_3$] | Ti–O and Ti–N | Amorphous | 450 °C–750 °C |
| [CpTi(O$^i$Pr)$_3$] | Ti–O and Ti–C | Anatase | 450 °C |
| | | Anatase–rutile | 550 °C |
| | | Rutile | 650 °C |
| | | | 750 °C |
| [Ti(O$^i$Pr)$_4$] | Ti–O | Anatase | 450 °C–550 °C |
| | | Anatase–rutile | 650 °C–750 °C |
| [Bu$^t$OTi(O$^i$Pr)$_3$] | Ti–O | Anatase | 450 °C |
| | | Anatase–rutile | 550 °C–750 °C |

As expected, the grains grew larger at higher temperatures, however the coalescence of individual crystallites was less pronounced, which manifested as more complex nanostructured landscapes and higher surface roughness (Fig. 5 (a)–(d)). The columnar arrangements of smaller units observed in the cross-sectional SEM image of the TiO$_2$ coating obtained at 650 °C confirmed the above hypothesis (Fig. 5 (e)). Evaluation of film growth rates (Fig. 6) achieved using precursors **1–6** at 550 °C revealed lowest deposition rates, determined by cross-sectional SEM analyses of several samples for [(Me$_3$Si)$_2$NTi(O$^i$Pr)$_3$] (5 nm min$^{-1}$) whereas manifold higher growth rates (up to 140 nm min$^{-1}$) were obtained using



**Fig. 5** SEM images showing morphology evolution in CVD-grown TiO$_2$ films obtained at (a) 450 °C, (b) 550 °C, (c) 650 °C and (d) 750 °C using [CpTi(O$^i$Pr)$_3$; (e) representative cross-sectional SEM image of a film obtained with [CpTi(O$^i$Pr)$_3$] on Si at 650 °C.

precursors, which exclusively contained Ti–O bonds (Fig. 6). This is suggestive of differential decomposition pathways for the precursor species and surface reactions at 550 °C. Nevertheless, the heteroleptic precursors offered better control over phase selectivity and homogeneous morphology, which are important parameters to control the functional behaviour of inorganic films.



**Fig. 4** SEM images illustrating the influence of deposition temperature on the TiO$_2$ morphology using [ClTi(O$^i$Pr)$_3$] at (a) 450 °C, (b) 550 °C and (c) 650 °C in a LPCVD process.



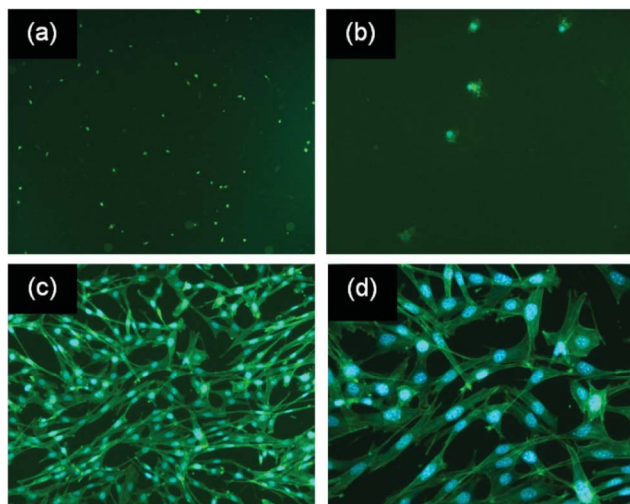**Fig. 6** Growth rates of TiO$_2$ films obtained using different Ti precursors at 550 °C on silicon(100) substrate.

**Fig. 7** Optical microscope images of osteoblast cells cultivated on TiO$_2$ surfaces grown using precursor [ClTi(O$^i$Pr)$_3$] (a, b) and [CpTi(O$^i$Pr)$_3$] (c, d) at 550 °C showing different patterns of cell growth and proliferation rates.

Investigations on the biocompatible properties of the TiO$_2$ coatings were performed by studying *in vitro* cell attachment of MC3T3-E1 osteoblasts as well as the resulting cell-growth and adhesion behaviour on titanium oxide surfaces. Analysis of the cell growth showed that deposits obtained using [ClTi(O$^i$Pr)$_3$], [Et$_2$NTi(O$^i$Pr)$_3$] and [(Me$_3$Si)$_2$NTi(O$^i$Pr)$_3$] were not favourable for cell growth, whereas films obtained using [Ti(O$^i$Pr)$_4$] and [CpTi(O$^i$Pr)$_3$] exhibited enhanced growth of the osteoblasts.

To investigate the biocompatibility and potential cytoxicity (due to eventual release of metal ions or presence of heteroatoms), bone cells (osteoblasts) were cultivated on anatase surfaces grown with different morphologies using [ClTi(O$^i$Pr)$_3$]; in both the cases little cell vitality was observed, which was evident in the spherical morphology of osteoblasts formed on these surfaces (Fig. 7 (a) and (b)). The presence of traces of chlorine emerging from the precursor composition might be responsible for the limited bio-response of these films as the phase structure (anatase) did not change at different growth temperatures. Highly faceted titania deposited by thermolysis of [Et$_2$NTi(O$^i$Pr)$_3$] (Fig. S3, ESI†) and amorphous titanium oxide layers formed by and CVD of [(Me$_3$Si)$_2$NTi(O$^i$Pr)$_3$] (Fig. S5) showed no cell activity at all which can be attributed to the presence of heteroelements and secondary phases, which are not bio-conducive. The highest level of cell attachment and proliferation activity, evident in higher growth rates together with pronounced intercellular links forming tissue like structures, was observed on TiO$_2$ deposits obtained from [CpTi(O$^i$Pr)$_3$] as shown in Fig. 7 (c) and (d). We also observed high osteoblast affinity for titania coatings derived from CVD of [Ti(O$^i$Pr)$_4$], however the proliferation and number of cells was lower than that observed for [CpTi(O$^i$Pr)$_3$] (Fig. S6, ESI†).

## Conclusions

Titanium dioxide (TiO$_2$) films of different phase compositions and surface topographies were grown using a molecule-based CVD process involving both homoleptic ([Ti(O$^i$Pr)$_4$]) and heteroleptic ([ClTi(O$^i$Pr)$_3$], [Et$_2$NTi(O$^i$Pr)$_3$], [(Me$_3$Si)$_2$NTi(O$^i$Pr)$_3$], [CpTi(O$^i$Pr)$_3$] and [Bu$^t$OTi(O$^i$Pr)$_3$]) compounds. The film morphologies ranged from smooth amorphous coatings to highly faceted crystalline microstructures. Both the phase constitution (amorphous, anatase or rutile) and grain structure of the films varied markedly depending on the deposition temperatures (450–750 °C), whereas the composition was entirely governed by the precursor configuration and decomposition behaviour. In summary, the chemical design of titanium precursors modulated the phase and surface texture of TiO$_2$ films by adjusting the deposition parameters, which in turn influenced the bioactivity of the nanostructured surfaces.

Our preliminary results of cell growth on TiO$_2$ surfaces show that cell adhesion and growth behaviour is modulated by a number of parameters such as chemical composition, impurities and microarchitecture. All aforementioned parameters could be modulated by the chemically designed molecular precursors and could be used to tune the biofunctional response at the cell-surface interface.

## Acknowledgements

## Notes and references

1 K. L. Choy, *Prog. Mater. Sci.*, 2003, **48**, 57–170.
2 W. Yang and C. A. Wolden, *Thin Solid Films*, 2006, **515**, 1708–1713.
3 B. Karunagaran, K. Kim, D. Mangalaraj, J. Yi and S. Velumani, *Sol. Energy Mater. Sol. Cells*, 2005, **88**, 199–208.
4 J. Y. Zhang, I. W. Boyd, B. J. O'Sullivan, P. K. Hurley, P. V. Kelly and J. P. Senateur, *J. Non-Cryst. Solids*, 2002, **303**, 134–138.
5 B. Kim, D. Byun, J. K. Lee and D. Park, *Jpn. J. Appl. Phys.*, 2002, **41**, 222–226.
6 R. Gerbasi, M. Bolzan, N. El Habra, G. Rossetto, L. Schiavi, A. Strini and S. Barison, *J. Electrochem. Soc.*, 2009, **156**, K233–K237.
7 B. Huber, A. Brodyanski, M. Scheib, A. Orendorz, C. Ziegler and H. Gnaser, *Thin Solid Films*, 2005, **472**, 114–124.
8 C. H. Heo, S.-B. Lee and J.-H. Boo, *Thin Solid Films*, 2005, **475**, 183–188.
9 Y. Sun, *Appl. Surf. Sci.*, 2004, **233**, 328–335.

10 (a) J. Huaxia, C. B. Ponton and P. M. Marquis, *J. Mater. Sci.: Mater. Med.*, 1992, **3**, 283; (b) R. Z. LeGeros and J. P. LeGeros, in *An Introduction to Bioceramics*, ed. L. L. Hench and J. Wilson, World Scientific, Singapore, 1993; (c) B. Li, X. Liu, C. Cao and C. Ding, *J. Biomed. Mater. Res. A*, 2007, **83**(4), 23; (d) X. Liu, X. Zhao, R. K. Fu, J. P. Ho, C. Ding and P. K. Chu, *Biomaterials*, 2005, **26**(31), 6143.

11 M. P. Casaletto, G. M. Ingo, S. Kaciulis, G. Mattogno, L. Pando and G. Scavia, *Appl. Surf. Sci.*, 2001, **172**, 167.

12 N. Moritz, S. Areva, J. Wolke and T. Peltola, *Biomaterials*, 2005, **26**, 4460–4467.

13 L. Xie, G. Yin, D. Yan, X. Liao, Z. Huang, Y. Yao, Y. Kang and Y. Liu, *J. Mater. Sci.: Mater. Med.*, 2010, **21**, 259–266.

14 J. Lausmaa, B. Kasemo and H. Mattsson, *Appl. Surf. Sci.*, 1990, **44**, 133–146.

15 B. D. Ratner, *J. Biomed. Mater. Res.*, 1993, **27**, 837–850.

16 F. Variola, J. H. Yi, L. Richert, J. D. Wuest, F. Rosei and A. Nanci, *Biomaterials*, 2008, **29**, 1285–1298.

17 G. Zhao, Z. Schwartz, M. Wieland, F. Rupp, J. Geis-Gerstorfer, D. L. Cochran and B. D. Boyan, *J. Biomed. Mater. Res., Part A*, 2005, **74A**, 49–58.

18 F. Variola, F. Vetrone, L. Richert, P. Jedrzejowski, J. H. Yi, S. Zalzal, S. Clair, A. Sarkissian, D. F. Perepichka, J. D. Wuest, F. Rosei and A. Nanci, *Small*, 2009, **5**, 996–1006.

19 D. D. Deligianni, N. Katsala, S. Ladas, D. Sotiropoulou, J. Amedee and Y. F. Missirlis, *Biomaterials*, 2001, **22**, 1241–1251.

20 F. Vetrone, F. Variola, P. T. de Oliveira, S. F. Zalzal, J. H. Yi, J. Sam, K. F. Bombonato-Prado, A. Sarkissian, D. F. Perepichka, J. D. Wuest, F. Rosei and A. Nanci, *Nano Lett.*, 2009, **9**, 659–665.

21 (a) S. Mathur, S. Barth and H. Shen, *Chem. Vap. Deposition*, 2005, **11**, 11–16; (b) S. Mathur and S. Barth, *Small*, 2007, **3**, 2070–2075.

22 R. Mueller, F. Hernandez-Ramirez, H. Shen, H. Du, W. Mader and S. Mathur, *Chem. Mater.*, 2012, **24**(21), 4028–4035.

23 J. M. Lackner and W. Waldhauser, *J. Adhes. Sci. Technol.*, 2010, **24**, 925–961.

24 A. Sherman, *Jpn. J. Appl. Phys.*, 1991, **30**, 3553–3557.

25 K. S. Yeung and Y. W. Lam, *Thin Solid Films*, 1983, **109**, 169–178.

26 M. Veith, A. Altherr and H. Wolfanger, *Chem. Vap. Deposition*, 1999, **5**, 87–90.

27 S. Mathur, H. Shen, V. Sivakov and U. Werner, *Chem. Mater.*, 2004, **16**, 2449–2456.

28 S. Mathur and P. Kuhn, *Surf. Coat. Technol.*, 2006, **201**, 807–814.